Binary Protein Adsorption on Gel-Composite Ion-Exchange Media

Rebecca Karst Lewus and Giorgio Carta
Dept. of Chemical Engineering, University of Virginia, Charlottesville, VA 22903

The adsorption kinetics of mixtures of lysozyme and cytochrome-C on S-HyperD-M, a cation exchanger composed of a rigid macroporous silica matrix whose pores are filled with a functionalized polyacrylamide gel, was characterized. Single-component isotherms were found to follow approximately the steric mass-action law of Brooks and Cramer, and an extension of this model to a binary system was consistent with two-component uptake equilibrium results. Transient adsorption experiments were done to investigate the kinetics of sequential and simultaneous adsorption of the two proteins. At low protein concentrations, adsorption is essentially noncompetitive, and mass transfer is controlled by the external film resistance. At higher concentrations, equilibrium becomes competitive and coupling of the intraparticle diffusion fluxes occurs. A model based on a Maxwell–Stefan approach, where the driving force for diffusion is expressed in terms of the chemical potential gradient, was in approximate agreement with the experimental results.

Introduction

In general, a description of the rate of mass transfer is needed for the design, optimization, and scale-up of adsorptive separation processes since in many of these applications the process performance is mass-transfer-limited (LeVan et al., 1997). Mass transfer is especially important in preparative and process-scale separations of proteins since these molecules have low diffusivities. In the case of ion-exchange media, for example, since the kinetics of adsorption is normally rapid, diffusional limitations typically determine the time scales for batch adsorption and are the dominant mechanism of band broadening in chromatographic separations (Yamamoto et al., 1988).

A number of studies have been previously dedicated to protein mass transfer in both porous and gel-type ion-exchange matrices. However, previous studies have only considered mass transfer under either nonadsorbing or noncompetitive, weakly binding conditions (e.g., Davies, 1989; Bloomingburg et al., 1991; Boyer and Hsu, 1992; Coffman et al., 1997) or have been limited to the adsorption or desorption of a single protein (e.g., Graham and Fook, 1982; Tsou and Graham et al., 1985; Graham et. al., 1987; Kopaciewicz et al., 1987; Skidmore et al., 1990; Bloomingburg and Carta, 1994; Yoshida et al., 1994). Multicomponent mass transfer under competitive adsorption conditions is, however, obviously important in many applications. Nevertheless, while there have been some theoretical analyses (e.g., Hossain and Do, 1987), there have been no published reports of multicomponent protein mass-transfer measurements in ion exchangers for these conditions.

In previous work (Fernandez and Carta, 1996; Fernandez et al., 1996; Weaver and Carta, 1996; Lewus et al., 1998), we have characterized the single-component equilibria and rates of adsorption and desorption for several proteins on commercially available gel-composite media known as HyperD (BioSepra, Inc., Marlborough, MA). These materials are obtained by incorporating a functionalized polyacrylamide gel in the pores of a rigid matrix. The gel provides ion-exchange sites for protein adsorption, while the rigid matrix provides structural strength. As a result, these materials are characterized by high binding capacity and can be used at elevated flow rates of the mobile phase. Mass-transfer rates in these materials are affected by either the external mass-transfer resistance or by intraparticle diffusion or by a combination of both, depending on the protein concentration and the solution ionic strength. Thus, as shown previously, a model ac-

Correspondence concerning this article should be addressed to G. Carta.

counting for both resistances is generally needed to describe mass transfer in these systems.

In this work, we extend the measurements of protein mass transfer in these gel-filled media to multicomponent situations. Experimental data are obtained in stirred-batch and shallow-bed contactors using lysozyme and cytochrome-C as model proteins. Two types of conditions are considered. In the first, the two proteins are simultaneously adsorbed from dilute solutions; in this case, the two proteins codiffuse to and within the ion exchanger. In the second case, the process is carried out sequentially; one of the two proteins is adsorbed first followed by exposure of the protein-loaded ion exchanger to a solution containing the other protein. In this case, the two proteins counterdiffuse to reach a final equilibrium concentration. A model taking into account the external mass-transfer resistance and the coupling of diffusion fluxes in the adsorbent medium through a Maxwell–Stefan approach is developed to describe the rates of mass transfer. The experiments conducted are representative of the kinetics that would be encountered in the frontal analysis or displacement chromatography separations of mixtures of the two proteins. Thus, the results of the analysis are expected to be useful in predicting *a priori* the performance of fixed-bed separations.

Experimental

Materials

The ion-exchange medium used in this work was S-HyperD-M (BioSepra, Inc., Marlborough, MA). This material is based on highly porous polystyrene-coated silica particles whose pores are filled with a functionalized polyacrylamide gel. The S-form of the material possesses a strong cation exchange functionality. The silica backbone has a porosity value of 0.65 (value supplied by the manufacturer), and the hydrated particles have a density of 1.424 g/cm^3 (Weaver and Carta, 1996). The volume-average diameter of the particle sample used was 78 μm. The particles were pretreated as discussed by Weaver and Carta (1996).

The model proteins used in this work, chicken egg-white lysozyme ($M_r = 14{,}400$, pI = 11) and cytochrome-C from bovine heart ($M_r = 13{,}300$, pI = 10.6), were obtained from Sigma Chemical Co. (St. Louis, MO). All other chemicals used were purchased from either Sigma Chemical Co. or Fisher Scientific (Pittsburgh, PA). All experiments were performed at room temperature (23 ± 2°C) in a 10-mM Na_2HPO_4 aqueous buffer adjusted to a pH of 6.5 with acetic acid. At this pH, both lysozyme and cytochrome-C carry a net positive charge.

It should be noted that cytochrome-C absorbs visible light as well as ultraviolet light and has a particularly strong absorbance at the wavelength of 405 nm. Lysozyme, on the other hand, absorbs only ultraviolet light and has essentially no absorbance at 405 nm. As a result, as shown by Bloomingburg et al. (1991), it is possible to determine the concentration of both proteins in a mixture by measuring simultaneously the absorbance at 405 and in the UV region.

Equilibrium measurements

Uptake isotherms for lysozyme at various salt concentrations in the range 0–1000 mM were obtained previously in our laboratory (Lewus et al., 1998), while those for cytochrome-C were obtained in this work. In these experiments, 5-cm^3 samples of protein solutions of known concentration were equilibrated with approximately 0.05 cm^3 of hydrated HyperD media at each desired salt concentration in glass vials that were capped and rotated gently for several hours. When equilibrium was reached (as indicated by the fact that there was no further variation in absorbance), the supernatant from each vial was sampled and its concentration determined via spectrophotometric analysis at 405 nm. The following mass balance was used to calculate the total amount of protein adsorbed:

$$q_i = \frac{V}{V_M}\left(C_i^0 - C_i\right), \tag{1}$$

where q_i is the amount of protein adsorbed (mg/cm^3 of media); V is the volume of solution (cm^3); V_M is the volume of media (cm^3); and C_i^0 and C_i are the initial and equilibrium protein concentrations (mg/cm^3 of solution), respectively.

Since the total water content of the media samples used varied slightly from run to run, the results were expressed in terms of the volume of hydrated particles. To obtain this volume, the moisture content (determined by drying at 120°C) and the known density of the media were used.

Transient adsorption and desorption experiments

Transient adsorption experiments were conducted with equipment similar to that used by Lewus et al. (1998). Both stirred-batch and shallow-bed experiments were done. In the stirred-batch experiments a sample of the HyperD media was suspended in an agitated vessel and the protein concentration was monitored over time. A glass vessel, 5 cm in diameter and 7 cm tall and equipped with a Teflon-coated magnetically driven impeller with 4-cm flat blades, operated at 300 rpm, was used.

Two absorbance monitors (Pharmacia Biotech, Piscataway, NJ, Mod. UV-1) in series were used to continuously track the concentration of the protein solution at wavelengths of 254 and 405 nm. A stream of the protein solution, drawn through a 10-μm stainless-steel frit (Upchurch Scientific, Oak Harbor, WA), was continuously circulated through these monitors with a Cole-Parmer (Niles, IL) peristaltic pump at a flow rate of 22 cm^3/min. Based on the calculated volume of tubing, frits, and monitors, the residence time in the monitoring loop was estimated to be less than 5 s. Prior to the experiments, the system was calibrated by measuring the absorbance of pure cytochrome-C and lysozyme solutions of known concentration at both wavelengths. As expected, there was no detectable absorbance at 405 nm for lysozyme. Thus, for mixtures of the cytochrome-C and lysozyme, the concentration of cytochrome-C could be obtained directly from the absorbance at this wavelength. The contribution of cytochrome-C to the absorbance at 254 nm could then be found and subtracted from the absorbance at 254 nm in order to determine the absorbance of the lysozyme. Finally, the concentration of lysozyme could be calculated from this absorbance value using a calibration curve. As in the batch

equilibrium experiments, the amount of protein adsorbed at a given time was determined from Eq. 1.

In the sequential adsorption experiments, the particles were added to 80 cm^3 of a cytochrome-C solution preloaded in the vessel and allowed to reach equilibrium (~ 1500 s). A 20-cm^3 volume of a lysozyme solution, sufficiently concentrated to attain the desired initial lysozyme concentration upon addition to the original solution, was then rapidly added to the vessel, and the concentration of both proteins was followed to a new equilibrium state. In the coadsorption experiments, a sample of the clean S-HyperD-M media was added to 100 cm^3 of a solution containing both proteins that had previously been placed in the vessel.

Shallow-bed experiments were also carried out to determine the rate of adsorption and desorption with a constant bulk protein concentration and for hydrodynamic conditions similar to those that could be found in a column operated at high flow rates of the mobile phase. The apparatus is described by Lewus et al. (1998) and consists of a shallow-bed column made by packing a small sample of S-HyperD-M media between two layers of Q-HyperD-M media (BioSepra, Inc., Marlborough, MA) in a 5-mm-ID glass column (Pharmacia Biotech, Piscataway, NJ, Mod. HR 5/2). The Q-HyperD-M media has the same particle-size distribution as the S-form; however, it has a strong anion-exchange functionality rendering it inert to the positively charged proteins. Experimentally, we observed that there was no detectable uptake of cytochrome-C by the Q-HyperD media for these conditions, and previous work (Lewus, et al., 1998) showed that the same is true for lysozyme. Thus, it appears that any adsorption of these two proteins by Q-HyperD is hindered by their strong net positive charge at this pH. Consequently, it was used only to provide support to the S-HyperD layer and ensure a good flow distribution. The volume of the S-HyperD-M particles in the shallow bed was determined to be 0.00374 cm^3 using the method described by Lewus et al. (1998). A ProSys Chromatography Workstation (BioSepra, Inc.) is used in conjunction with the shallow-bed assembly. Three of the pumps in this unit are used to supply constant flows of protein and buffer solutions and a Valco multiport valve (Valco Instrument Co., Inc., Houston, TX) is used to allow for rapid switching of flows at the shallow-bed entrance.

In order to determine the adsorption rate of cytochrome-C, the protein solution was fed to the shallow-bed column for a known length of time. A buffer solution was then sent through the column briefly in order to rinse off unbound protein in the interstices. Finally, a 500-mM NaCl solution was used to desorb the protein from the adsorbent. The amount of cytochrome-C that was adsorbed during the time of loading was determined by finding the area under the elution curve and converting it to mass of protein using a calibration curve. The two-component adsorption–desorption experiments were run in a similar manner, except that the shallow-bed bed was initially loaded with cytochrome-C until it was saturated. Then, a solution of lysozyme was fed to the column to desorb the cytochrome-C. The amount of cytochrome-C desorbed at a specific time was found by integrating the elution curve up to that time. Protein solutions containing 1.0 and 2.0 mg/cm^3 of lysozyme were used for the desorption step. The flow rate in these experiments was 4 cm^3/min. The ProSys unit software was used for all area integrations.

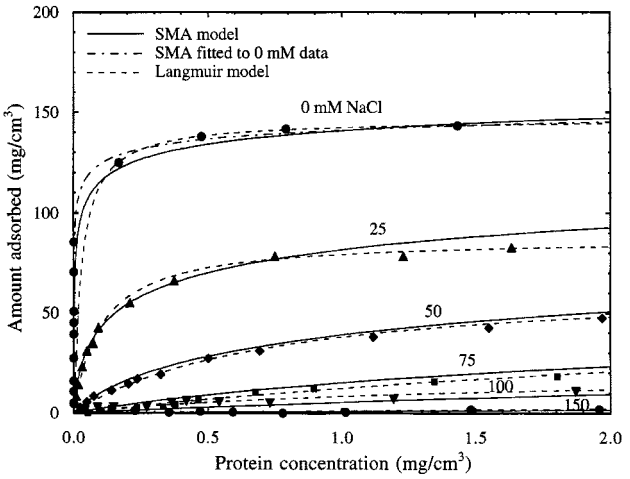

Figure 1. Equilibrium isotherms for cytochrome-C with different NaCl concentrations.

SMA model lines are calculated with the parameters in Table 1.

Results and Analysis

Uptake equilibrium

Single-component isotherms for cytochrome-C and lysozyme are shown in Figures 1 and 2 at different salt concentrations over the range 0 to 150 mM in a 10-mM Na_2HPO_4 aqueous buffer at pH 6.5. The uptake equilibrium is very favorable for both proteins at low salt concentrations and becomes more linear as the salt concentration is increased. However, the maximum uptake observed for lysozyme with no added NaCl is nearly 70% greater than that observed for cytochrome-C. The dependence of equilibrium uptake on salt concentration is also much more pronounced for cytochrome-C than for lysozyme. In fact, at 150-mM NaCl, uptake of cytochrome-C by the media is barely detectable, while the uptake of lysozyme at this salt concentration is still quite large. Since the two proteins have a similar molecular weight and shape, these differences cannot be ascribed solely to size-exclusion or surface coverage effects. As discussed in previous work (Fernandez and Carta, 1996; Weaver and Carta, 1996; Lewus et al., 1998), protein adsorption in HyperD media is dependent on the partitioning of these molecules between the solution phase and the charged gel that fills the pores of the rigid matrix. As a result, the uptake behavior is dependent both on the characteristic charge of the proteins and on their ability to interact effectively with multiple ion-exchange sites within the three-dimensional network of the polymer gel.

Two commonly used empirical models were used in this work to represent the equilibrium data: the Langmuir model and the steric mass-action model (SMA) developed by Brooks and Cramer (1992). The first model is given by

$$C_i = \frac{q_i}{b_i(q_{m,i} - q_i)}, \qquad (2)$$

where $q_{m,i}$ and b_i are, in general, salt-dependent parameters.

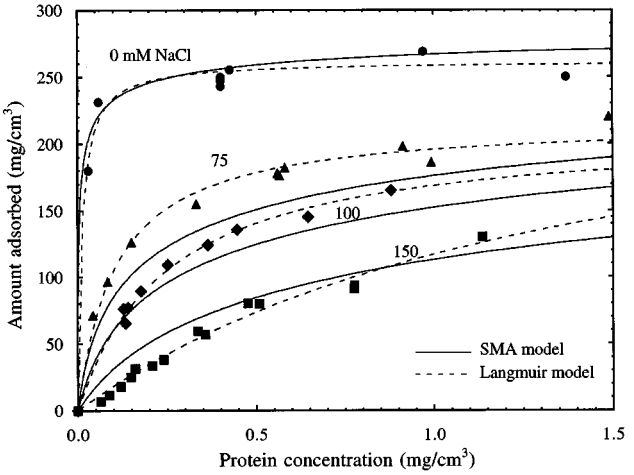

Figure 2. Equilibrium uptake isotherms for lysozyme with different NaCl concentrations.

Experimental data and Langmuir lines are from Lewus et al. (1998). SMA model lines are calculated with the parameters in Table 1.

The SMA model is given by

$$C_i = \frac{q_i C_I^{z_i}}{K_i\left[q_0 - (z_i + \sigma_i) q_i\right]^{z_i}}, \tag{3}$$

where C_I is the ion concentration (Na^+ in this case), q_0 is the equivalent ion-exchange capacity of the adsorbent medium; and K_i is an affinity coefficient. This model is based on the assumption that a protein molecule i undergoes ion exchange with z_i functional groups while simultaneously hindering further exchange on σ_i groups, and contains an explicit dependence on salt concentration. Thus, since q_0 can be determined independently for a given ion exchanger, only the three species-dependent parameters K_i, z_i, and σ_i are needed to represent equilibrium data over a range of salt concentrations.

A comparison of the isotherm fits obtained with these equations is shown in Figures 1 and 2. In each case, the model parameters were determined by a nonlinear fit, except for q_0, which was obtained from the manufacturer. A summary of these parameters is given in Table 1. The z-value determined for cytochrome-C is close to those reported by other authors (Brooks and Cramer, 1992; Gallant et al., 1996). The value of z for lysozyme, however, is smaller than the value reported by Gallant et al. (1996) but similar to values reported by Whitley et al. (1989). In our work, the lower z_i-value and the higher affinity constant for lysozyme are consistent with the greater capacity and smaller dependence on salt concentration that was observed experimentally. In general, a somewhat more accurate fit was obtained with the Langmuir model. However, this model required a different set of values of $q_{m,i}$ and b_i at each salt concentration. Conversely, for cytochrome-C, the SMA model provided a reasonable fit of the data using only three parameters over the entire salt concentration range. The results for lysozyme were not as good, as seen in Figure 2. Thus, greater weight was given to the 0-mM NaCl data in this fit, since the rate measurements were done for these conditions. The SMA isotherms for cytochrome-C at 0-mM NaCl are also shown for comparison in Figure 1. The values of K_i, z_i, and σ_i obtained in this case were 1.4, 5.7, and 10.8, respectively. The values of z_i and σ_i are close to the original ones. However, the value of K_i considerably larger, yielding a better fit at very low concentrations.

Table 1. SMA Equilibrium Parameters for S-HyperD-M at pH 6.5*

Parameter	Cytochrome-C	Lysozyme
z_i	5.7	2.8
σ_i	9.1	7.9
K_i	0.20	210

*$q_0 = 220\ \mu$eq/cm^3.

An advantage of the SMA model is that it can be extended in a straightforward manner to multicomponent adsorption (Gallant et al., 1996). For the case of a two-component system, the following equations are obtained:

$$C_i = \frac{q_i}{K_i}\left(\frac{C_I}{\bar{q}_I}\right)^{z_i} \tag{4}$$

$$\bar{q}_I = q_0 - \sum_{j=1}^{2}(z_j + \sigma_j) q_j = q_0 - \sum_{j=1}^{2}(z_j + \sigma_j) K_j C_j \left(\frac{\bar{q}_I}{C_I}\right)^{z_j}, \tag{5}$$

where $\bar{q}_I$ is the concentration of functional groups available for ion exchange at each protein loading level. A limited number of two-component equilibrium data was obtained by allowing the transient batch experiments to continue until equilibrium was reached. Representative results are shown in Table 2 in comparison with predictions from Eqs. 4 and 5 using the parameters obtained from the single-component fit. As seen in this table, at equilibrium simultaneous adsorption of the two proteins is observed only when the final concentration of lysozyme is very low. For other conditions, only lysozyme is adsorbed at equilibrium, indicating that this

Table 2. Two-Component Uptake Equilibrium Data for S-HyperD-M in 10-mM Na_2HPO_4 Buffer at pH 6.5 Compared with SMA Model Predictions*

C_{CC}^0 (mg/cm^3)	C_{LYO}^0 (mg/cm^3)	C_{CC}^{final} (mg/cm^3)	C_{LYO}^{final} (mg/cm^3)	q_{CC}^{exp} (mg/cm^3)	q_{CC}^{pred} (mg/cm^3)	q_{LYO}^{exp} (mg/cm^3)	q_{LYO}^{pred} (mg/cm^3)
0.2	0.2	0.032	0.022	62	60	64	75
1.0	0.2	0.50	0.030	105	99	63	68
1.0	1.0	1.0	0.35	~ 0	~ 0	250	260

*CC = cytochrome-C; LYO = lysozyme.

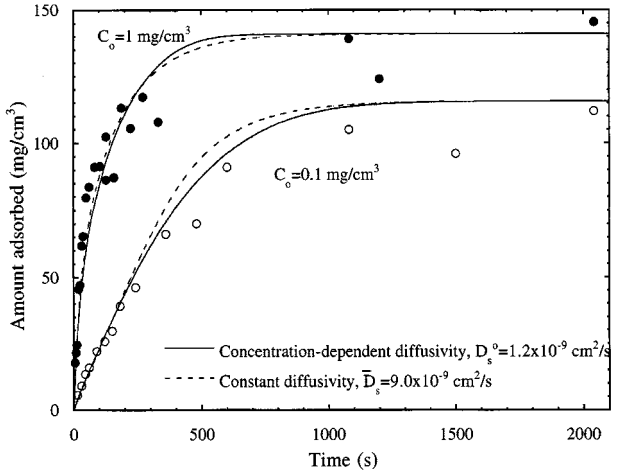

Figure 3. Single-component shallow-bed uptake kinetics for cytochrome-C.

Model lines are calculated with $k_{f,i} = 0.0029$ cm/s, with equilibrium parameters from Table 1. [NaCl] = 0 mM.

species acts as an effective competitive displacer of cytochrome-C. The SMA model appears to capture the essence of this experimental behavior, suggesting that this model can be used for correlating and predicting the transient uptake behavior for single- and two-protein adsorption/desorption conditions. The most significant deviations are expected to occur at very low concentrations where the steepness of the isotherm prevents accurate measurements.

Single-component uptake kinetics

The transient uptake kinetics of cytochrome-C and lysozyme on clean S-HyperD-M in the shallow-bed contactor are shown in Figures 3 and 4 for two different protein concentrations. Previous work on HyperD (Fernandez and Carta, 1996; Weaver and Carta, 1996; Lewus et al., 1998) has shown that mass-transfer rates in these materials are consistent with a diffusional mechanism where the driving force is expressed in terms of the adsorbed protein concentration gradient. In fact, if a fluid phase concentration is used as the driving force, effective pore diffusivities higher than the free solution diffusivity are needed to fit the data (Weaver and Carta, 1996). In this case, mass-transfer rates for these conditions are potentially affected by two resistances in series: the external resistance in the boundary layer surrounding the particles and the intraparticle diffusional resistance. As shown, for example, by Fernandez and Carta (1996) and Weaver and Carta (1996), the relative importance of these two resistances is determined by the group:

$$\delta = \frac{1}{5}\,\frac{k_{f,i} r_p}{\bar{D}_{s,i}}\,\frac{C_i}{q_i^*}, \tag{6}$$

where $k_{f,i}$ is the film coefficient; r_p is the particle radius; and $\bar{D}_{s,i}$ the average intraparticle diffusivity. The quantity C_i/q_i^* is the partition ratio that depends on the solution concentration, C_i, and the corresponding equilibrium concentration in the particle, q_i^*. Values of $\delta \ll 1$ indicate a dominance of the external resistance, while values of $\delta \gg 1$ indicate a dominance of intraparticle diffusional limitations. It should be noted that, since the isotherm is nearly rectangular for the conditions of these experiments, q_i^* is relatively constant and the value of δ changes essentially in proportion to C_i.

The following equations and boundary conditions were used to model the single-component transient uptake:

$$\frac{\partial q_i}{\partial t} = \frac{1}{r^2}\,\frac{\partial}{\partial r}\left(-r^2 J_i\right) \tag{7}$$

$$J_i = -D_{s,i}\,\frac{\partial q_i}{\partial r} \tag{7a}$$

$$r = 0, \qquad \frac{\partial q_i}{\partial r} = 0 \tag{7b}$$

$$r = r_p, \qquad J_i = -k_{f,i}\left(C_i - C_i^s\right) \tag{7c}$$

$$t = 0, \qquad q_i = q_i^0, \tag{7d}$$

where C_i^s is the solute concentration at the particle surface. To compare this model with the experimental results, the film coefficient, $k_{f,i}$, can be estimated from correlations (LeVan et al., 1997). Alternatively, it can be fitted to initial uptake-rate data at a protein concentration sufficiently low to render $\delta \ll 1$. With regard to the intraparticle diffusivity, $D_{s,i}$, there are two possibilities. The first is to assume that $D_{s,i}$ is a constant in Eq. 7, and thus determine an average value $\bar{D}_{s,i}$ by fitting the data. The second possibility is to assume a functional form for the concentration dependence of the intraparticle diffusivity. Currently, no theory is available to predict *a priori* the diffusivity of a cationic macromolecule in an anionic gel, such as that contained in S-HyperD, or its concentration dependence. As a consequence, a semiempirical scheme, based on the Maxwell–Stefan approach, was adopted where the intraparticle diffusion flux is expressed in terms of the chemical potential of the adsorbed solute. An approach

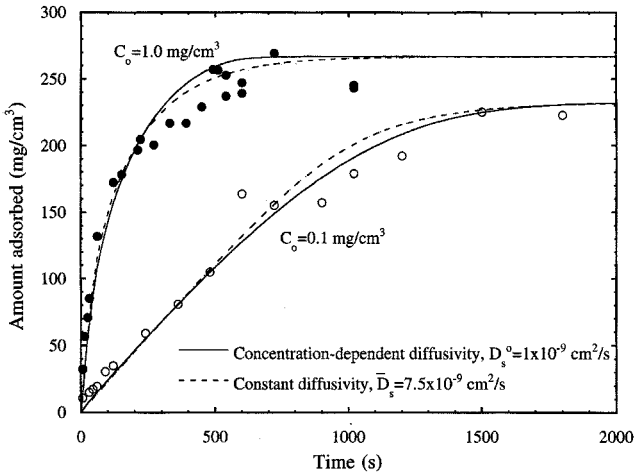

Figure 4. Single-component shallow-bed uptake kinetics for lysozyme.

Experimental data are from Lewus et al. (1998). Model lines are calculated with $k_{f,i} = 0.0029$ cm/s, with equilibrium parameters from Table 1. [NaCl] = 0 mM.

of this type has been used to describe single- and multicomponent micropore diffusion in zeolites (Garg and Ruthven, 1972; Kärger and Bülow, 1975), activated carbon (Seidel and Carl, 1989), and carbon molecular sieves (Chen and Yang, 1992), as well as to describe protein transport in membranes (Robertson and Zydney, 1988). According to this approach, the diffusion flux of a species i can be written as (Ruthven 1984; Krishna and Wesselingh, 1997):

$$J_i = - q_i \frac{D^0_{s,i}}{RT} \frac{\partial \mu_i}{\partial r}, \tag{8}$$

where μ_i is the chemical potential and $D^0_{s,i}$ is the Maxwell–Stefan diffusivity. In the adsorption literature (Ruthven, 1984; Yang, 1987; LeVan et al., 1997), the latter is also referred to as the ''corrected diffusivity.'' The relationship between $D^0_{s,i}$ and $D_{s,i}$ is readily found, since for an ideal solution $\mu_i = \mu^0_i + RT \ln C_i$. Using the chain rule of differentiation, the following result is obtained for the flux:

$$J_i = - D^0_{s,i} \frac{q_i}{C_i} \frac{dC_i}{dq_i} \frac{\partial q_i}{\partial r}, \tag{9}$$

where the derivative dC_i/dq_i is calculated from the uptake isotherm. For the SMA equilibrium model, the following result is obtained:

$$J_i = - D^0_{s,i} \frac{q_0 + (z_i - 1)(z_i + \sigma_i) q_i}{q_0 - (z_i + \sigma_i) q_i} \frac{\partial q_i}{\partial r}, \tag{10}$$

which gives the concentration dependence of the intraparticle diffusivity in terms of the equilibrium parameters q_0, z_i, and σ_i. It should be noted that this neglects the electrical coupling of diffusion fluxes within the ion exchanger. Since the degree to which electrostatic coupling and electrolyte invasion is important in HyperD is uncertain, this factor is neglected in the analysis. However, it is interesting to note that if the classic Nernst–Planck treatment of diffusion in ion exchange (Helfferich, 1962) is applied to the counterdiffusion of a charged protein and a small counterion, a result mathematically equivalent to Eq. 10 is obtained, provided that the diffusivity of the protein in the gel can be assumed to be much smaller than that of the counterion.

A comparison of calculated and experimental results for single-component uptake is shown in Figures 3 and 4. The curves shown are calculated using either Eq. 7a with $D_{s,i} = \overline{D}_{s,i}$ for the constant diffusivity case, or using Eq. 10 for the case of concentration-dependent diffusivity. In both cases, the film coefficient was assumed to be constant and found to be 0.0029 cm/s from the initial slope of the uptake curves at 0.1 mg/cm^3 protein concentration. Calculated curves were obtained from the numerical solution of the model using a finite-difference scheme similar to that used by Kataoka et al. (1977). $\overline{D}_{s,i}$ and $D^0_{s,i}$ were used as adjustable parameters and fitted to the high-concentration runs. As seen in Figures 3 and 4, both models provide adequate fits of the experimental results, and using the fitted values of $\overline{D}_{s,i}$ and $k_{f,i}$, it is possible to verify that the criterion for external mass-transfer control at the 0.1-mg/cm^3 protein concentration is satisfied. Interestingly, similar values of $\overline{D}_{s,i}$ and $D^0_{s,i}$ are found from the data fit for cytochrome-C and lysozyme, even though the uptake capacities for the two proteins are very different.

Two-component adsorption–desorption kinetics

Sequential adsorption experiments were conducted in both the shallow-bed and in the stirred-batch apparatus. The results for shallow-bed experiments are shown in Figure 5. In this case, the particles were initially loaded with a 1 mg/cm^3 cytochrome-C solution and then exposed to solutions containing 1 or 2 mg/cm^3 of lysozyme. The amount of cytochrome-C desorbed as a function of time was monitored as discussed previously and is shown in Figure 5. Clearly, the rate of desorption of cytochrome-C for these conditions is independent of the lysozyme concentration, as this species completely displaces cytochrome-C from the media.

The results for sequential adsorption experiments conducted in the stirred-batch apparatus are shown in Figure 6a–6d for different combinations of the initial cytochrome-C loading and the initial lysozyme concentration. In each experiment the adsorption of both cytochrome-C and lysozyme were monitored over time. In Figure 6a, both the initial cytochrome-C loading and the initial concentration of lysozyme were small. Little desorption of cytochrome-C occurs, as competition between the two proteins is very modest for these conditions. In Figure 6b, the initial cytochrome-C loading was high (close to the maximum) but a low initial lysozyme concentration was again used. In this case, there is a more pronounced desorption of cytochrome-C and a final equilibrium state is reached where again both proteins are adsorbed. In Figure 6c, both the initial cytochrome-C loading and the initial lysozyme concentration were high. In this case, the system approaches equilibrium gradually as a result of the slow

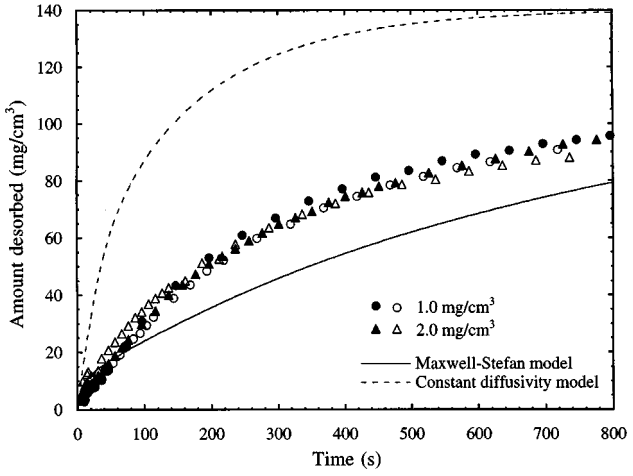

Figure 5. Shallow-bed desorption of cytochrome-C by exposure to solutions containing 1 and 2 mg/cm^3 of lysozyme.

Experimental results are given for two different runs at each lysozyme concentration. Lines are calculated $k_{f,CC} = k_{f,LYO} = 0.0029$ cm/s using $\overline{D}_{s,CC} = 9.0 \times 10^{-9}$ and $\overline{D}_{s,LYO} = 7.5 \times 10^{-9}$ cm^2/s for the constant diffusivity model, and $\overline{D}^0_{s,CC} = 1.2 \times 10^{-9}$ and $\overline{D}_{s,LYO} = 1.0 \times 10^{-9}$ cm^2/s for the concentration-dependent diffusivity model. $q^0_{CC} = 140$ mg/cm^3, [NaCl] = 0 mM.

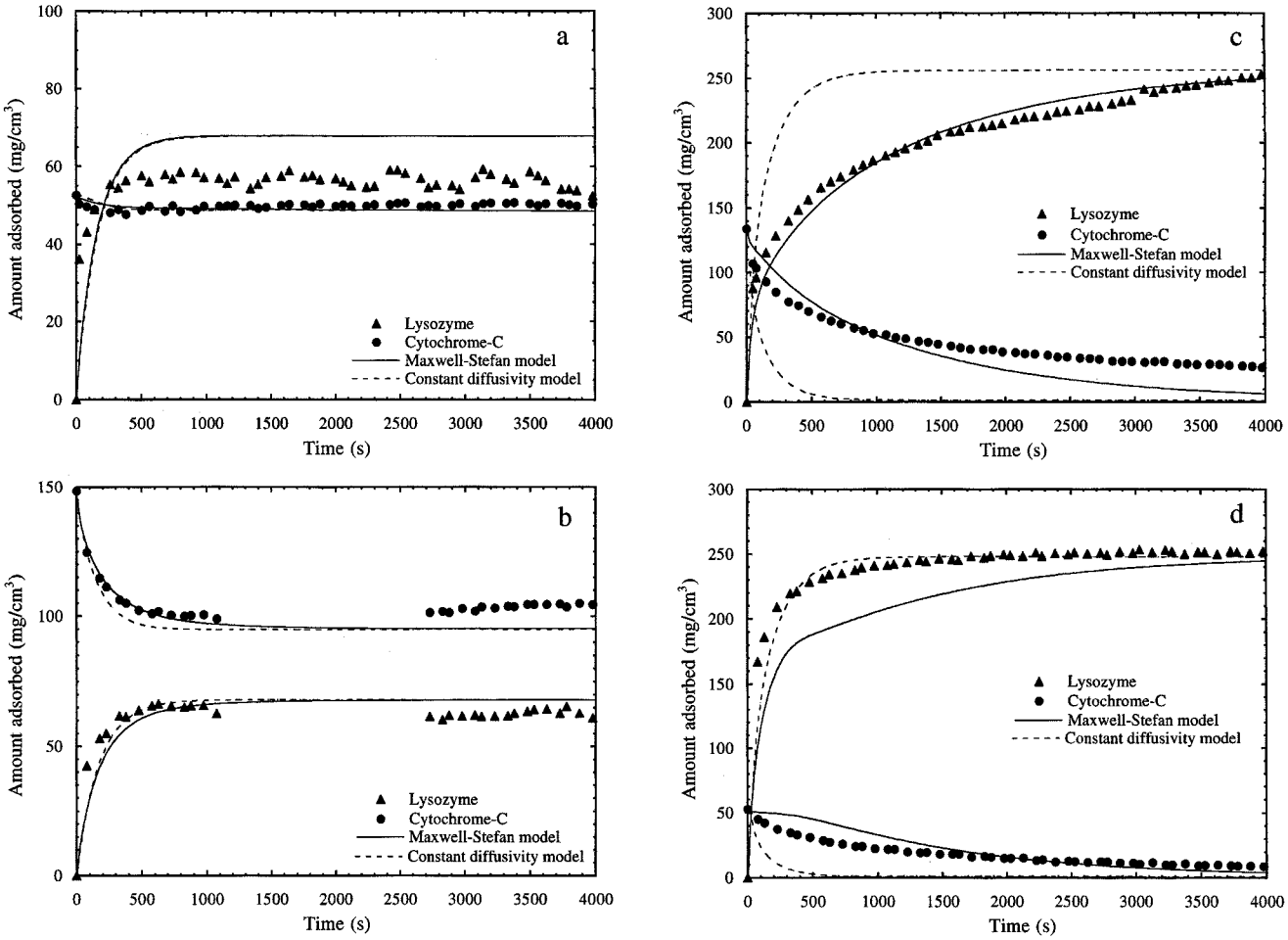

Figure 6. Batch desorption of cytochrome-C by exposure to lysozyme solutions.

Lines are calculated with $k_{f,CC} = k_{f,LYO} = 0.0026$ cm/s, using $\overline{D}_{s,CC} = 9.0\times10^{-9}$ and $\overline{D}_{s,LYO} = 7.5\times10^{-9}$ cm^2/s for the constant diffusivity model, and $D^0_{S,CC} = 1.2\times10^{-9}$ and $D^0_{s,LYO} = 1.0\times10^{-9}$ cm^2/s for the concentration-dependent diffusivity model. [NaCl] = 0 mM. (a) $q^0_{CC} = 50$, $C^0_{LYO} = 0.2$ mg/cm^3; (b) $q^0_{CC} = 150$, $C^0_{LYO} = 0.2$ mg/cm^3; (c) $q^0_{CC} = 130$, $C^0_{LYO} = 1.2$ mg/cm^3; (d) $q^0_{CC} = 50$, $C^0_{LYO} = 1.0$ mg/cm^3.

counterdiffusion of cytochrome-C and lysozyme in the particles. Eventually an equilibrium state is reached where essentially all the previously loaded cytochrome-C is desorbed. Finally, Figure 6d shows the results for the case where the initial cytochrome-C loading was small while the initial lysozyme concentration was high. Here lysozyme is adsorbed rapidly for short times. Desorption of the previously loaded cytochrome-C, however, occurs more slowly until eventually all of the cytochrome-C is desorbed.

Results for simultaneous adsorption experiments on clean S-HyperD-M particles in the stirred-batch apparatus are shown in Figure 7a–7c. In the first case (Figure 7a), the initial concentration was low for both proteins. For these conditions, the adsorption is essentially noncompetitive and the rate of mass transfer can be expected to be largely controlled by the external film resistance. In the second case, shown in Figure 7b, the cytochrome-C concentration was raised to 1 mg/cm^3 while keeping a low lysozyme concentration. In this case, there is an initial rapid rise of the cytochrome-C loading followed by a gradual decline toward the final equilibrium value. The lysozyme loading, on the other hand, simply rises to the final equilibrium value. The "overshoot" of the cytochrome-C-loading above the final equilibrium value is further accentuated when the concentration of both proteins is increased to 1 mg/cm^3. This case is illustrated in Figure 7c. For these conditions, both proteins are initially rapidly adsorbed. The loading of cytochrome-C, however, begins to decline gradually after about 200 s, as this species diffuses outward while lysozyme continues to be adsorbed. For long times ($t \sim 50{,}000$ s, data not shown), eventually all of the cytochrome-C that was adsorbed during the initial phase of contact was desorbed, while the lysozyme loading approached values corresponding to those for a pure lysozyme solution.

In order to predict the adsorption and desorption behavior in this system it is necessary to simultaneously take into account equilibrium and rate phenomena, considering both intraparticle and external transport limitations. As for the single-component case, two alternatives were considered: one using constant intraparticle diffusivities and one using the Maxwell–Stefan approach. In both cases, the external resistance is accounted for with a film coefficient. For the constant-diffusivity case, Eqs. 7 and 7a–7d are written for each component and integrated simultaneously. For the

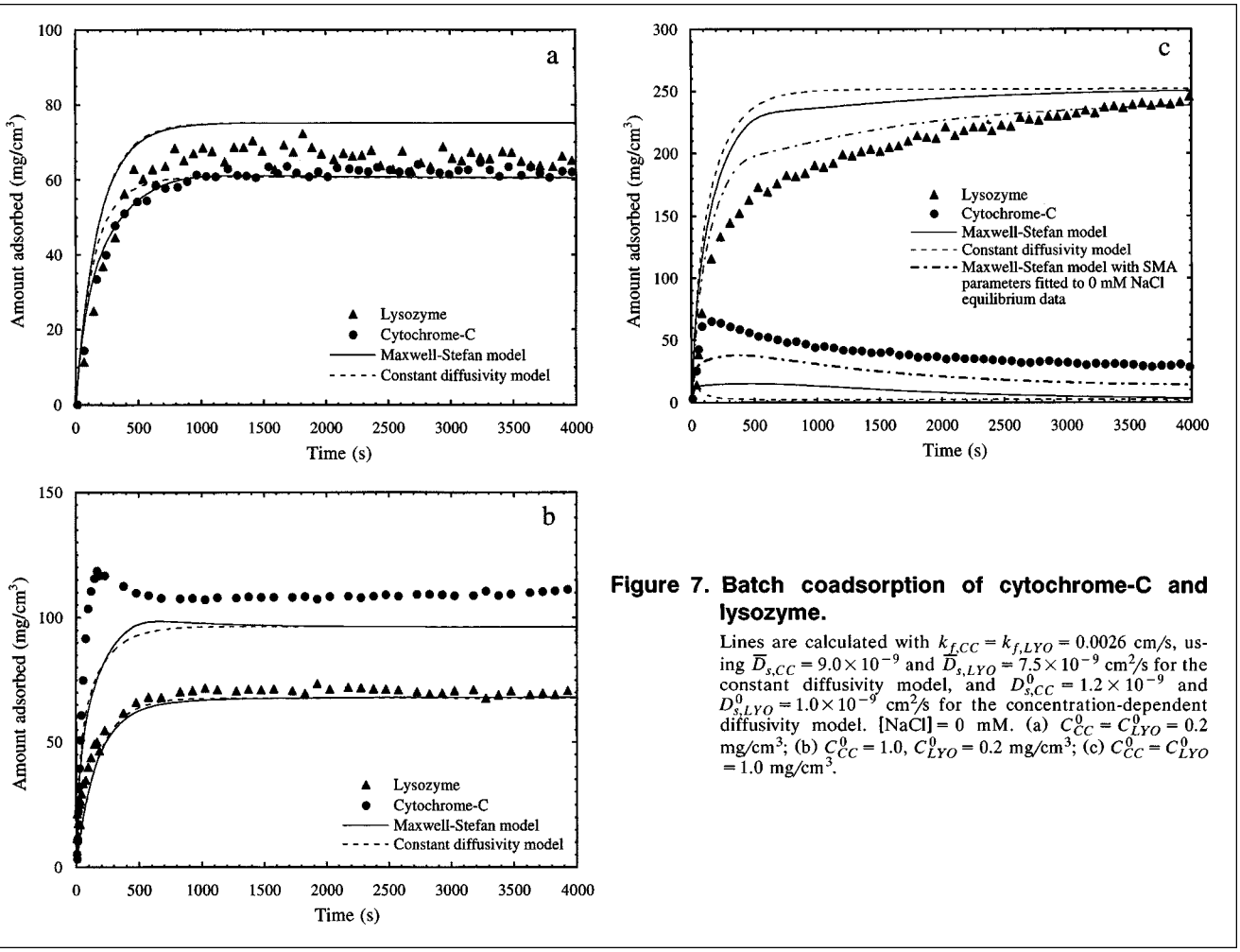

Figure 7. Batch coadsorption of cytochrome-C and lysozyme.

Lines are calculated with $k_{f,CC} = k_{f,LYO} = 0.0026$ cm/s, using $\bar{D}_{s,CC} = 9.0\times10^{-9}$ and $\bar{D}_{s,LYO} = 7.5\times10^{-9}$ cm^2/s for the constant diffusivity model, and $D^0_{s,CC} = 1.2\times10^{-9}$ and $D^0_{s,LYO} = 1.0\times10^{-9}$ cm^2/s for the concentration-dependent diffusivity model. [NaCl] = 0 mM. (a) $C^0_{CC} = C^0_{LYO} = 0.2$ mg/cm^3; (b) $C^0_{CC} = 1.0$, $C^0_{LYO} = 0.2$ mg/cm^3; (c) $C^0_{CC} = C^0_{LYO} = 1.0$ mg/cm^3.

Maxwell–Stefan approach, however, the fluxes are coupled as the chemical potential of each species is affected by the concentration of the other. The treatment adopted here is analogous to that used for adsorption in micropores (Round et al., 1966; Krishna and Wesselingh, 1997). Following Round et al., neglecting cross-terms in the chemical potential driving force, we obtain the following expressions for a two-component system

$$J_1 = -D^0_{s,1}\frac{q_1}{C_1}\left(\frac{\partial C_1}{\partial q_1}\frac{\partial q_1}{\partial r} + \frac{\partial C_1}{\partial q_2}\frac{\partial q_2}{\partial r}\right) \tag{11}$$

$$J_2 = -D^0_{s,2}\frac{q_2}{C_2}\left(\frac{\partial C_2}{\partial q_1}\frac{\partial q_1}{\partial r} + \frac{\partial C_2}{\partial q_2}\frac{\partial q_2}{\partial r}\right) \tag{12}$$

where the partial derivatives $\partial C_i/\partial q_i$ with $i, j = 1, 2$ are evaluated from the isotherm. Using the SMA model (Eqs. 4–5), the following equations are obtained

$$J_1 = -\left(D_{1,1}\frac{\partial q_1}{\partial r} + D_{1,2}\frac{\partial q_2}{\partial r}\right) \tag{13}$$

$$J_2 = -\left(D_{2,1}\frac{\partial q_1}{\partial r} + D_{2,2}\frac{\partial q_2}{\partial r}\right) \tag{14}$$

where

$$D_{1,1} = D^0_{s,1}\frac{\bar{q}_I + z_1(z_1+\sigma_1)q_1}{\bar{q}_I} \tag{15a}$$

$$D_{1,2} = D^0_{s,1}\frac{z_1(z_2+\sigma_2)q_1}{\bar{q}_I} \tag{15b}$$

$$D_{2,1} = D^0_{s,2}\frac{z_2(z_1+\sigma_1)q_2}{\bar{q}_I} \tag{15c}$$

$$D_{2,2} = D^0_{s,2}\frac{\bar{q}_I + z_2(z_2+\sigma_2)q_2}{\bar{q}_I} \tag{15d}$$

As the protein loading approaches zero, the $D_{i,i}$-terms, given by Eqs. 15a and 15d, approach the corresponding $D^0_{s,i}$-values, while the cross-terms in the diffusivity matrix $D_{i,j}$ given by

Eqs. 15b and 15c, vanish. At finite loadings, the fluxes become coupled and the concentration gradient of one species affects the flux of the other. These equations were used in conjunction with the particle conservation equations (Eqs. 7 and 7d–7d) and with an overall mass balance for the stirred-batch system. The latter is given by:

$$\frac{dC_i}{dt} = -\frac{3k_{f,i}}{r_p}\frac{V_M}{V}\left(C_i - C_i^s\right). \tag{16}$$

The equations were integrated numerically using a finite difference scheme as previously discussed. The value $k_{f,i} = 0.0026$ cm/s determined by Weaver and Carta (1996) for similar conditions was used in the computations.

The behavior predicted by these equations for sequential adsorption experiments is shown in Figures 5 and 6, and that predicted for coadsorption is shown in Figure 7. Numerical results are shown for both the case of constant diffusivities and for coupled fluxes. In general, it appears that predictions based on the Maxwell–Stefan approach are much closer to the experimental results than those based on the assumption that the diffusivities are constant. In experiments at low protein concentrations (e.g., Figures 6a and 7a), there is little difference between the two models, and both are in substantial agreement with the experimental results. This occurs because the rate for these conditions is determined to a large extent by the external resistance. The greatest differences are seen for the cases of sequential adsorption with high protein concentrations (e.g., Figures 5, 6c and 6d), where counterdiffusion of the two proteins results in lower rates than predicted, assuming constant diffusivities. In these cases, the Maxwell–Stefan-based model provides a reasonable prediction of the experimental behavior.

Finally, we can consider the coadsorption behavior shown in Figures 7a–7c. In this case, predictions from the Maxwell–Stefan model and from the constant-diffusivity model are similar. This likely occurs because the effects of coupling of diffusion fluxes are more pronounced when the two proteins counterdiffuse than when they diffuse in the same direction. In both cases, the agreement between model and experimental results is only qualitative. Nevertheless, the model provides some insight in the origin of the observed behavior by considering predicted concentration profiles at different times. Predicted profiles are shown in Figure 8a and 8b for conditions corresponding to those of Figure 7c. The figures show the intraparticle concentrations multiplied by the factor $(r/r_p)^2$ to better reflect the amount of each protein adsorbed at different radial positions. The figures also show the concentrations in the external film. For short times (Figure 8a, $t = 20$ s), the lysozyme concentration in the fluid phase immediately adjacent to the particle surface is very small, as the external resistance is dominant for this species for these conditions, thereby allowing a significant uptake of cytochrome-C. For longer times, however, the further uptake of lysozyme displaces the adsorbed cytochrome-C, some of which diffuses back to the solution phase and some toward the center of the particle. As the process continues, however, the external resistance becomes less and less important and the solution concentrations of the two proteins at particle surface approach the bulk values (see Figure 8b, $t = 500$ s). For these conditions, any previously adsorbed cytochrome-C tends to be completely displaced by lysoyzme. This, however, occurs gradually while the two species counterdiffuse in the ion exchanger.

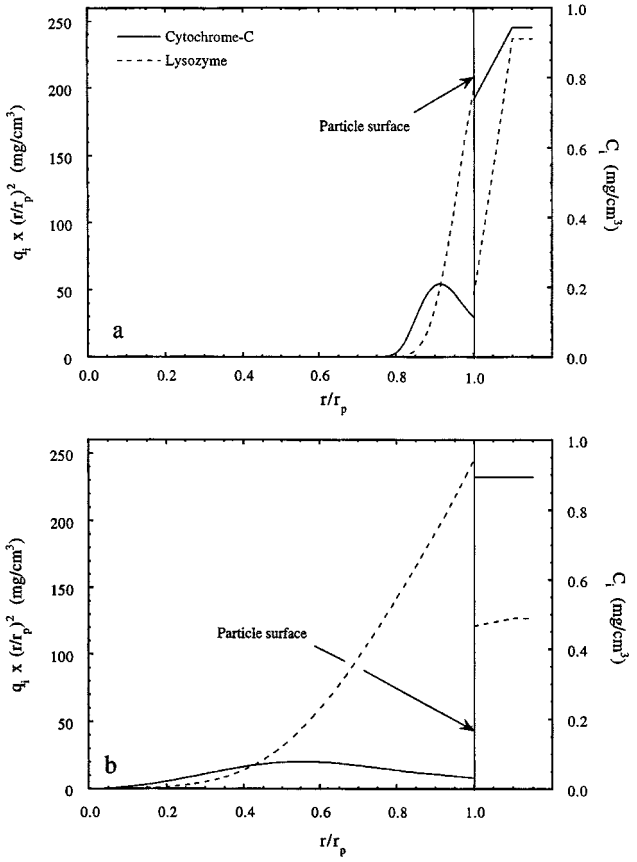

Figure 8. Concentration profiles predicted by Maxwell–Stefan model for coadsorption of cytochrome-C and lysozyme for conditions corresponding to those in Figure 7c.

It used $k_{f,CC} = k_{f,LYO} = 0.0026$ cm/s, $D^0_{s,CC} = 1.2\times10^{-9}$, and $D^0_{s,LYO} = 1.0\times10^{-9}$ cm^2/s. (a) $t = 20$ s; (b) $t = 500$ s. External concentrations are given as a reference.

The maximum cytochrome-C loading attained in the experiment in Figure 7c is only qualitatively predicted by the model. Inaccuracies in describing the competitive uptake equilibrium are, likely, responsible for the difference. To assess the effects of the equilibrium isotherm for these conditions, the SMA-model parameters fitted to the 0-mM NaCl data were used for the calculations. These parameters did not provide a good representation of the data at other salt concentrations, but accurately fitted the data with no salt. As shown in Figure 7c, predictions of the coadsorption behavior using the Maxwell–Stefan approach are closer to the experimental results using these parameters. It should be noted, however, that with the original equilibrium parameters, while the overshoot is not predicted in a quantitative manner, the gradual rate of decline in cytochrome-C loading that follows the overshoot is adequately predicted by the Maxwell–Stefan-based model. This decline is, conversely, predicted to be extremely

rapid using the constant-diffusivity description of intraparticle mass transfer.

Significance of Conclusions

We have measured the rates of adsorption and desorption for a two-protein system in an ion-exchanger medium designed for process-scale separations with the goal of establishing an approach for predicting multicomponent mass transfer in batch systems and adsorption columns for conditions where adsorpion is favorable and competitive.

A successful prediction of mass-transfer rates for these conditions requires (1) a description of competitive multicomponent protein-adsorption equilibrium; (2) a description of the external-boundary-layer resistance; and (3) a description of intraparticle diffusion rates. For the model system considered in this work, we have found that the SMA model of Brooks and Cramer (1992) provides an approximate description of single-protein uptake equilibria at different salt concentrations and is qualitatively consistent with two-component data. In particular, the SMA model predicts the cytochrome-C displacement by lysozyme in a manner consistent with the experiments. A rate expression based on a film coefficient is found to be adequate to describe the boundary-layer resistance. Accounting for this resistance is important for our system when the protein solution concentration is low. This resistance is likely responsible for the overshoot in cytochrome-C loading observed for short times in coadsorption experiments. Finally, with regard to the intraparticle transport rates, we found that a model taking into account the coupling of diffusion fluxes is needed to obtain a reasonable prediction of two-component mass transfer from single-component measurements. The effects of coupling are particularly important in sequential adsorption experiments at high protein loading, where intraparticle counterdiffusion of the two species is dominant. A Maxwell–Stefan approach where mass-transfer rates are proportional to the chemical-potential gradient appears to provide a useful framework for the description of these effects. Uncertainties in predicting multicomponent equilibria, variations in the Maxwell–Stefan diffusivities with protein loading, and electrical coupling of diffusion fluxes could affect the accuracy of these predictions. In general, however, predictions based on this approach appear to be more consistent with the experimental trends than predictions made assuming constant intraparticle diffusivities.

Acknowledgment

This research was supported by NSF Grant No. CTS-9709670. We gratefully acknowledge the gift of S- and Q-HyperD samples and of a ProSys unit by BioSepra, Inc.

Notation

J_i = diffusion flux, mg/cm^2·s or μmol/cm^2·s
q_i^0 = initial protein concentration in adsorbent medium, mg/cm^3 or μmol/cm^3
r = radial coordinate, cm
R = gas law constant, J/mol·K
t = time, s
T = temperature, K
z_i = characteristic charge parameter in SMA model, Eq. 3.
μ_i^0 = reference chemical potential, J/mol
σ_i = steric hindrance parameter in SMA model, Eq. 3

Literature Cited

Bloomingburg, G. F., J. S. Bauer, G. Carta, and C. H. Byers, "Continuous Separation of Proteins by Annular Chromatography," *Ind. Eng. Chem. Res.*, **29**, 1061 (1991).
Bloomingburg, G. F., and G. Carta, "Separation of Protein Mixtures by Continuous Annular Chromatography with Step Elution," *Chem. Eng. J.*, **55**, B19 (1994).
Boyer, P. M., and J. T. Hsu, "Experimental Studies in Restricted Protein Diffusion in Agarose Matrix," *AIChE J.*, **38**, 259 (1992).
Brooks, C. A., and S. M. Cramer, "Steric Mass-Action Ion Exchange: Displacement Profiles and Induced Salt Gradients," *AIChE J.*, **38**, 1969 (1992).
Chen, Y. D., and R. T. Yang, "Predicting Binary Fickian Diffusivities from Pure-Component Fickian Diffusivities for Surface Diffusion," *Chem. Eng. Sci.*, **47**, 3895 (1992).
Coffman, J. L., E. N. Lightfoot, and T. W. Root, "Protein Diffusion in Porous Chromatographic Media Studied by Proton and Fluorine PFG-NMR," *J. Phys. Chem. B.*, **101**, 2218 (1997).
Davies, P. A., "Determination of Diffusion Coefficients of Proteins in Beaded Agarose by Gel Filtration," *J. Chromatog.*, **483**, 221 (1989).
Fernandez, A. M., and G. Carta, "Charaterization of Protein Adsorption by Composite Silica-Polyacrylamide Gel Anion Exchangers: I. Equilibrium and Mass Transfer in Agitated Contactors," *J. Chromatog.*, **746**, 169 (1996).
Fernandez, A. M., W. S. Laughinghouse, and G. Carta, "Characterization of Protein Adsorption by Composite Silica-Polyacrylamide Gel Anion Exchangers: II. Mass Transfer in Packed Columns and Predictability of Breakthrough Behavior," *J. Chromatog.*, **746**, 185 (1996).
Gallant, S. R., S. Vunnum, and S. M. Cramer, "Modeling Gradient Elution of Proteins in Ion Exchange Chromatography," *AIChE J.*, **42**, 2511 (1996).
Garg, D. R., and D. M. Ruthven, "The Effect of the Concentration Dependence of Diffusivity on Zeolitic Adsorption Curves," *Chem. Eng. Sci.*, **27**, 417 (1972).
Graham, E. E., and C. F. Fook, "Rate of Protein Absorption and Desorption on Cellulosic Ion Exchangers," *AIChE J.*, **28**, 245 (1982).
Graham, E. E., A. Pucciani, and N. G. Pinto, "A Comparative Study of Models to Predict Protein Adsorption," *Biotechnol. Prog.*, **3**, 141 (1987).
Helfferich, F., *Ion Exchange*, McGraw-Hill, New York (1962).
Hossain, M. D. M., and D. D. Do, "Immobilization of Multienzyme in Porous Solid Supports—A Theoretical Study," *Chem. Eng. Sci.*, **42**, 255 (1987).
Kärger, J., and M. Bülow, "Theoretical Prediction of Uptake Behavior in Adsorption of Binary Gas Mixtures Using Irreversible Thermodynamics," *Chem. Eng. Sci.*, **30**, 893 (1975).
Kataoka, T., H. Yoshida, and Y. Ozasa, "Breakthrough Curve in Ion Exchange Column: Particle Diffusion Control," *J. Chem. Eng. Japan*, **10**, 385 (1977).
Kopaciewicz, W., S. Fulton, and S. Y. Lee, "Influence of Pore and Particle Size on the Frontal Uptake of Proteins—Implications for Preparative Anion-Exchange Chromatography," *J. Chromatog.*, **409**, 111 (1987).
Krishna, R., and J. A. Wesselingh, "The Maxwell-Stefan Approach to Mass Transfer," *Chem. Eng. Sci.*, **52**, 861 (1997).
LeVan, M. D., G. Carta, and C. M. Yon, "Adsorption and Ion Exchange," *Perry's Chemical Engineers' Handbook*, Sect. 16, D. W. Green, ed., McGraw-Hill, New York (1997).
Lewus, R. K., F. H. Altan, and G. Carta, "Protein Adsorption and Desorption on Gel-Filled Rigid Particles for Ion Exchange," *Ind. Eng. Chem. Res.*, **37**, 1079 (1998).
Robertson, B. C., and A. L. Zydney, "A Stefan-Maxwell Analysis of Protein Transport in Porous Membranes," *Sep. Sci. Technol.*, **23**, 1799 (1988).
Round, G. F., H. W. Habgood, and R. Newton, "A Numerical Analy-

sis of Surface Diffusion in a Binary Adsorbed Film,'' *Sep. Sci.*, **1**, 219 (1966).
Ruthven, D. M., *Principles of Adsorption and Adsorption Processes*, Wiley, New York (1984).
Seidel, A., and P. S. Carl, ''The Concentration Dependence of Surface Diffusion for Adsorption on Energetically Heterogeneous Adsorbents,'' *Chem. Eng. Sci.*, **44**, 189 (1989).
Skidmore, G. L., B. J. Horstmann, and H. A. Chase, ''Modeling Single-Component Protein Adsorption to the Cation Exchanger Sepharose FF,'' *J. Chromatog.*, **498**, 113 (1990).
Tsou, H.-S., and E. E. Graham, ''Prediction of Adsorption and Desorption of Protein on Dextran Based Ion-Exchange Resin,'' *AIChE J.*, **31**, 1959 (1985).
Weaver, L. E., and G. Carta, ''Protein Adsorption on Cation Exchangers: Comparison of Macroporous and Gel-Composite Media,'' *Biotechnol. Prog.*, **12**, 342 (1996).
Whitley, R. D., R. Wachter, F. Liu, and N.-H. L. Wang, ''Ion-Exchange Equilibria of Lysozyme, Myoglobin and Bovine Serum Albumin,'' *J. Chromatog.*, **465**, 137 (1989).
Yamamoto, S., K. Nakanishi, and R. Matsuno, *Ion Exchange Chromatography of Proteins*, Dekker, New York (1988).
Yang, R. T., *Gas Separation by Adsorption Processes*, Butterworth, Boston (1987).
Yoshida, H., M. Yoshikawa, and T. Kataoka, ''Parallel Transport of BSA by Surface and Pore Diffusion in Strongly Basic Chitosan,'' *AIChE J.*, **40**, 2034 (1994).

Manuscript received July 30, 1998, and revision received Dec. 2, 1998.